ARQII Publication
http://arqiipubl.com/ams
APPLICATIONS OF MODELLING AND SIMULATION
eISSN 2600-8084
VOL 8, 2024, 239-247

A Study of Savonius Wind Turbine Performance with Unsimilar Configuration of Concave and Convex Blade Sides

Abdel-Fattah Mahrous*

Mechanical Power Engineering Department, Menoufia University, 32511, Shebin El-Kom, Egypt

*Corresponding author: afmahrous@yahoo.com

Submitted 30 March 2024, Revised 17 July 2024, Accepted 27 July 2024, Available online 12 August 2024.

Abstract: Modifications in classical Savonius rotor have extensively been studied in an attempt to improve turbine performance. The present work investigates experimentally and computationally the effects of combining two different blade shape configurations into a single blade shape design on the Savonius rotor performance. The concave and convex sides of Savonius rotor blade were made unsimilar in shape. Three rotor blades differ in configuration were experimentally and computationally tested including the combined blade. The computational results were primarily validated against experimental data and accordingly a suitable turbulence model was chosen. Among few tested turbulence models, the realizable k-ε turbulence model showed closest agreement with the measured data. The results of turbine performance indicate that the combined blade shows better performance than other models particularly at higher tip speed ratios. The maximum power coefficient of the combined blade is increased by about 10% when compared with other investigated rotors. This may be attributed to the blade shape effects on the resulting total drag force. Increasing the maximum power coefficient in addition to the operational range of tip speed ratio are expected when running Savonius turbine with the combined blade.

Keywords: Blade shape; Combined blade; Computational fluid dynamics (CFD); Savonius rotor; Wind power.

1. INTRODUCTION

Numerous studies that make use of energy sources that are beneficial to the environment have extensively been carried out in an attempt to increase utilization of new and renewable energy sources. Such sources include, but are not limited to, wind, solar, biomass, ocean, and geothermal energy. Being abundant and easily found everywhere, wind energy is regarded as one of the renewable energy sources that is developing very quickly. A wind turbine is a device that is necessary to harness wind energy and converts it into electrical power. Wind turbines are classified, based on the disposition of axis of rotation, as horizontal axis wind turbine (HAWT) and vertical axis wind turbine (VAWT). Savonius turbine is a type of vertical axis wind turbine that is simple in construction. In its simplest form, it is formed from a pair of semi-circular buckets, or blades, connected to opposing sides of a vertical shaft, as shown in Figure 1. As airflow passes through the Savonius turbine, the rotor begins to spin because of the difference in drag forces between the advancing and returning blades. Due to this way of operation, the Savonius turbine is known as a drag type turbine. When compared to other types of rotor turbines, Savonius turbine has a low power coefficient. This highlights the significance of numerous studies that were conducted to improve the Savonius turbine's performance. Some of Savonius turbine distinguishing features are its rotation regardless of wind direction (omnidirectionality) and its capability to run at very low wind speeds.

Several attempts were made to modify the Savonius turbine design in order to increase the power coefficient and consequently improve the performance. This was accomplished, for instance, by introducing various geometrical elements outside the classical turbine rotor. The purpose of such elements is to increase the driving torque and/or to decrease the negative torque acting on the returning blade. Application of these designs includes introducing flow deflectors on the turbine rotor's upstream side [1-3], employing entry guiding plates [4] and providing wind boosters or curtains [5-7]. Modifying rotor blade geometry, on the other hand, was performed to enhance the power coefficient [8-14]. This modification includes blade shape and number, number of turbines stages, blade overlapping ratio, and incorporation of end plates.

The negative torque applied to the convex side of Savonius turbine returning blade is the main cause of reduction in the turbine power conversion efficiency. A great effort was made in an attempt to reduce negative drag through modifications in classical blade profile. Various drag reducing profiles of two-dimensional blade were reviewed in reference [15]. Considering

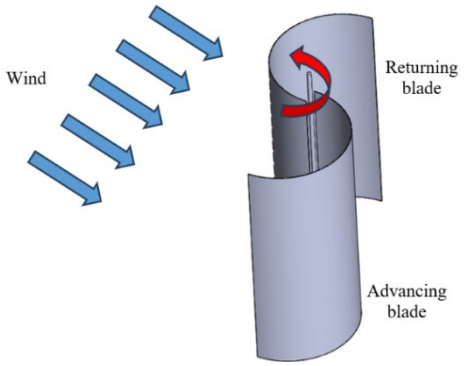

Figure 1. Two blades Savonius rotor.

modification on blade geometry, the Bach type blades [16-18] as well as the universal blade [9] showed higher power coefficients than the conventional blade. In addition, combining conventional blade with one of the modified blades showed better performance than the modified blade alone [19, 20]. The universal blade two-dimensional profile is created in such a way that the Blade Shape Factor (BSF), blade arm length to circular arc radius, varies in value from coordinate point to another [9]. By using the equation of point of tangency of blade arm with blade circular arc at different degrees of blade shape factor [9], the set of points that make up the blade geometry of the suggested modified Savonius blade was obtained.

This work aims to study computationally and experimentally the effects of blade shape design on the performance of Savonius turbine. In the current study, two different configurations of the two sides (inner concave and outer convex) of Savonius blade were combined in a single design in order to investigate their effect on turbine performance. The inner concave surface of the rotor blade was formed by a universal blade profile [9] while the outer convex surface is shaped as a Bach type blade profile with a specific blade shape factor. The performance of the single modified blade with combined surfaces was computationally and experimentally investigated and compared with the performance of similar blade sides configuration rotors.

2. WIND TURBINE TORQUE AND POWER CALCULATIONS

The primary function of the wind turbine's rotor blades is to transform the wind stream's kinetic energy into mechanical energy. Typically, torque and power coefficients are used to express the wind turbine's performance. The relationship between the mechanical power generated by the turbine's rotor and the power that is available in the wind as kinetic energy is known as the power coefficient (C_p). It is written as [9]:

$$C_p = \frac{P_R}{P_W} = \frac{2\omega T}{\rho A_s V^3} \tag{1}$$

where P_R is the rotor's produced mechanical power, P_W is the available wind power, ω is the rotor speed of rotation, T is the turbine rotor's torque, ρ is the air density, A_S is the rotor's swept area, and V is the speed of free stream wind. Equation (2) is used to get the wind turbine's torque coefficient (C_m).

$$C_m = \frac{4T}{\rho A_s V^2 D} \tag{2}$$

where D is the rotor diameter. The ratio of the tip speed of the rotor ($\omega D/2$) to the free stream wind speed is known as the wind turbine's tip speed ratio λ.

$$\lambda = \frac{\omega D}{2V} \tag{3}$$

3. EXPERIMENTAL METHODOLOGY AND TEST MODELS

In the real application of wind turbine, it is used to convert the natural wind power into mechanical work. However, the natural wind speed, and thus the power, varies and so artificial wind source producing constant wind speed has to be used to study the turbine performance. In the current study, a free jet test rig was used to experimentally investigate the wind turbine performance. The experimental setup of the free jet wind tunnel was formerly constructed in the Lab of Advanced Fluid Mechanics, Department of Mechanical Power Engineering, College of Engineering, Menoufia University [8, 21, 22].

The free jet wind tunnel, an isometric representation of which is displayed in Figure 2, mainly consists of a centrifugal fan (1) powered by an AC electrical motor (2). The wind speed is controlled by varying the electrical motor frequency which in turn results in a change in the fan impeller rotating speed and consequently the wind speed. Using an AC motor of 15 HP rated power and 1480 rpm, the maximum generated wind speed at the fan exit is about 13 m/s [8]. A circular cross-sectional area duct (3) of 1.1 m diameter and 1.5 m length is connected to the fan exit to guide the air flow towards the turbine. The circular duct is made from sheets of galvanized iron having a thickness of about 1.5 mm.

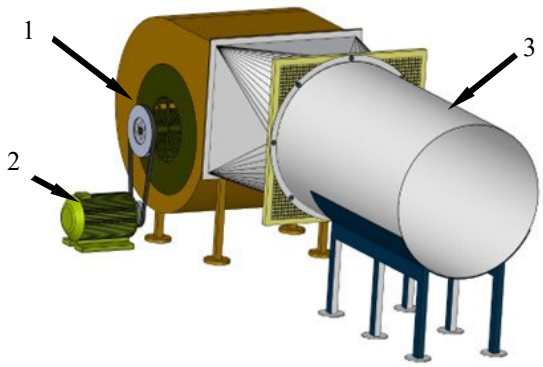

Figure 2. An isometrical illustration of the experimental setup of the free jet wind tunnel used in the present work: (1) Centrifugal fan, (2) Electrical motor, (3) Circular duct.

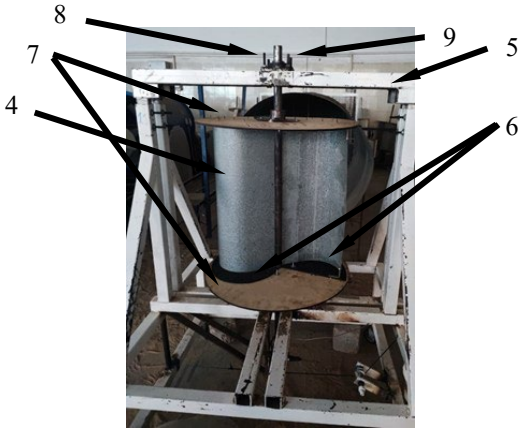

Figure 3. A photograph of an experimental Savonius test model used in the present work: (4) Savonius rotor, (5) Structural frame, (6) Guiding plates, (7) End plates, (8) Turbine shaft, (9) Bearing.

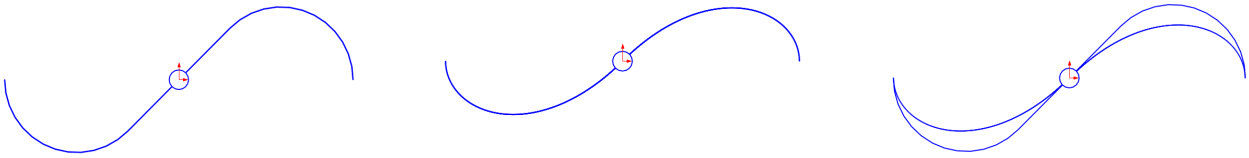

(a) (b) (c)

Figure 4. Investigated Savonius rotor test models: (a) Bach type rotor (BSF = 1 and Arc angle = 135º), (b) LIUB [9], (c) Combined blade, BSF type (convex side) - LIUB (concave side).

Figure 3 shows a photograph of the experimental Savonius test model used in the present work. A structural frame (5) made of mild steel plates houses the Savonius rotor (4), which is positioned in front of the fan exit circular duct at a specific distance. The approximate area of the Savonius rotor in the direction of wind is (54 cm x 60 cm). The blades of the rotor are made from galvanized iron material of thickness 0.5 mm by casting process. Working as guiding and supporting plates for rotor blades, two semicircular wooden layers (6), made from medium-density fiberboard wood of 5 mm thickness each and having blade shapes engrooved in each of them, are fabricated and fitted to the end sides of rotor blades. These supporting plates are then connected to the rotor upper and lower end plates (7) that are manufactured from wood of 6 mm thickness. A steel shaft of 30 mm diameter (8) connects the turbine rotor to the structural steel frame via the upper and lower end plates. Roller ball bearings (9) are mounted at the top and the bottom of the steel frame to allow smooth rotation of the Savonius rotor.

Connected to the turbine shaft by mechanical coupling, An RT2-USB torque transducer is used to measure the turbine generated mechanical torque and the rotational speed. For this purpose, a weighing pan and a nylon string with 1 mm diameter are used for recording the torque produced by the rotor. A digital Pitot-static tube is utilized to record the free stream wind speed. Upon positioning the wind turbine in a free jet flow, the wind speed is being unevenly distributed all over the frontal area of the turbine that is facing the air flow. By measuring the wind speed spatially (in both horizontal and vertical directions) along the rotor's projected region, one may determine the average value of the incoming wind speed. The mechanical torque on the rotating shaft as well as the shaft rotational speed are measured at various wind speeds and resistive load values in order to calculate the mechanical power produced by the turbine rotor. Data is acquired with the help of WinEasyTORK torque transducer software, version 1.6.

Three models of Savonius rotors were computationally and experimentally tested. Figure 4 illustrates the profiles of these models. The first model was a modified blade (the Bach type rotor) with a blade shape factor (BSF) of 1.0 and arc angle of 135º. The second one was the laterally inverted universal blade, LIUB, where its configuration can be referred to in reference [9]. The third one was a combined blade with its inner concave surface formed from the laterally inverted universal blade (LIUB) while its outer convex surface formed from the Bach type blade with a blade shape factor of 1.0. Having the same rotor diameter and height, the three models were computationally and experimentally tested with a turbine shaft and nearly zero overlap ratio.

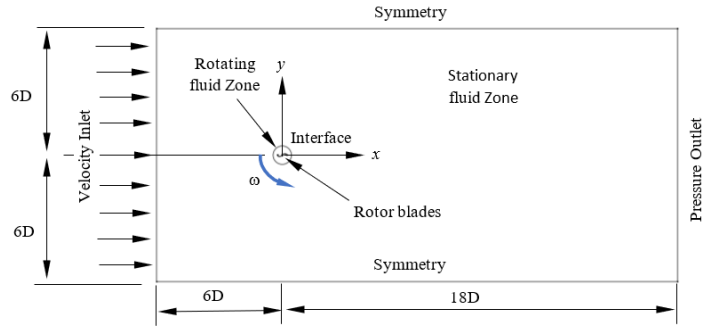

Figure 5. 2-D CFD domain with prescribed fluid zones and boundary conditions.

4. CFD METHODOLOGY AND CONDITIONS

In this section, the fluid flow governing equations and Computational Fluid Dynamics (CFD) conditions are presented. Here, the finite volume Computational Fluid Dynamics (CFD) ANSYS Fluent (Version 15) was used to computationally predict the performance of Savonius rotor with different blade configurations. The problem under investigation here is considered unsteady and the flow regime was turbulent. It was computationally solved in two-dimensional (2-D) domain. For turbulent flow, the fluid velocity and pressure are spatially and temporally fluctuating. To account for turbulence, fluctuations are averaged to form the so-called Reynolds Averaged Navier-Stokes (RANS) equations. The time-based RANS equations are expressed as follows [9, 23, 24].

Mass conservation equation:

$$\frac{\partial \rho}{\partial t} + \frac{\partial}{\partial x_j}(\rho u_j) = 0 \tag{4}$$

Momentum conservation equation:

$$\frac{\partial}{\partial t}(\rho u_j) + \frac{\partial}{\partial x_i}(\rho u_i u_j) = -\frac{\partial P}{\partial x_j} + \rho g_j + \frac{\partial}{\partial x_i}\left[\mu\left(\frac{\partial u_i}{\partial x_j} + \frac{\partial u_j}{\partial x_i}\right)\right] + \frac{\partial}{\partial x_i}\left(-\rho\overline{u_i' u_j'}\right) \tag{5}$$

Here, ρ is the air density, t is the time, u_j is the fluid velocity component in the direction j, P is the pressure, g is the acceleration due to gravity, μ is the coefficient of dynamic viscosity and x_i denotes the spatial coordinate. A suitable turbulence model has to be employed to model Reynolds's shear stress tensor, the term $u_i' u_j'$ in the momentum conservation equation (Equation 5).

The 2-D computational domain of the investigated problem along with the designated boundary conditions [9, 24] is illustrated in Figure 5. To take the advantage of sliding mesh concept in Ansys Fluent [23], the CFD domain was decomposed into two distinct fluid zones: namely the rotating and stationary fluid zones. These two zones are separated by interface boundaries and differ only in motion. Having a diameter of 2.0 times the rotor diameter (i.e. 2D), the rotating zone was set for the turbine rotor. The remaining area of the computational domain was defined as stationary fluid zone. A uniform velocity inlet boundary condition of 7 m/sec with a 5% turbulence intensity was assigned to the CFD domain left boundary. This boundary was set at an upstream distance of 6D before the center of turbine shaft. For the outlet boundary, a pressure outlet boundary condition of 1 standard atmosphere was defined. The pressure outlet boundary was located at a downstream distance of 18D from the rotor axis of rotation. Identified as symmetric boundary conditions, the top and lower planes were placed at a distance of 6D each.

SolidWorks CAD software was used to generate the geometry of wind turbine test models as well as the remining part of CFD domain. The turbine geometry was thereafter imported into ANSYS Meshing environment and discretized to obtain the proper 2-D mesh topology. For instance, Figure 6 depicts the computational mesh around as well as in the vicinity of the rotor of the combined Savonius wind turbine. Triangular mesh was used in the rotating zone, while a quad-tri hybrid mesh was chosen for the stationary zone. A 1.150 value for the mesh growth rate was set for the main grid. In the far field region, where the wind turbine rotor hardly affects the flow, a coarser mesh was employed. In order to accurately calculate the turbine torque and to get all physical effects within the rotating zone, the boundary mesh of the rotor blades needs to be extremely fine [25]. Figure 6 further displays a closer look at the computational grid in the vicinity of the rotor blade. To help in capturing the boundary layer region adjacent to the blade wall, 8 boundary mesh inflation layers were generated with a growth rate of 1.2 and a total depth of 0.0125D.

During the simulations, the SIMPLE method (Semi-Implicit Method) was selected to offer a better relationship between pressure and velocity. To apply mass conservation and determine the pressure field, this algorithm uses a relationship between velocity and pressure corrections [23]. Second order upwind spatial discretization in the pressure, momentum, and turbulence equations was used throughout the calculations along with the double precision pressure-based algorithm and a Least Squares Cell Based technique for gradients. At each turbine's angular velocity, the transient computations' time step was set equivalent to a one degree of rotor rotation [24, 26]. This value of time step was said to offer an independent time step solution [27]. The boundary conditions for solid walls were set as no-slip conditions for the velocity components and zero normal pressure gradients. Besides, all solid walls were assigned as smooth walls. To assess solution convergence, a 10^{-6} tolerance value for solution convergence was applied to the simulations.

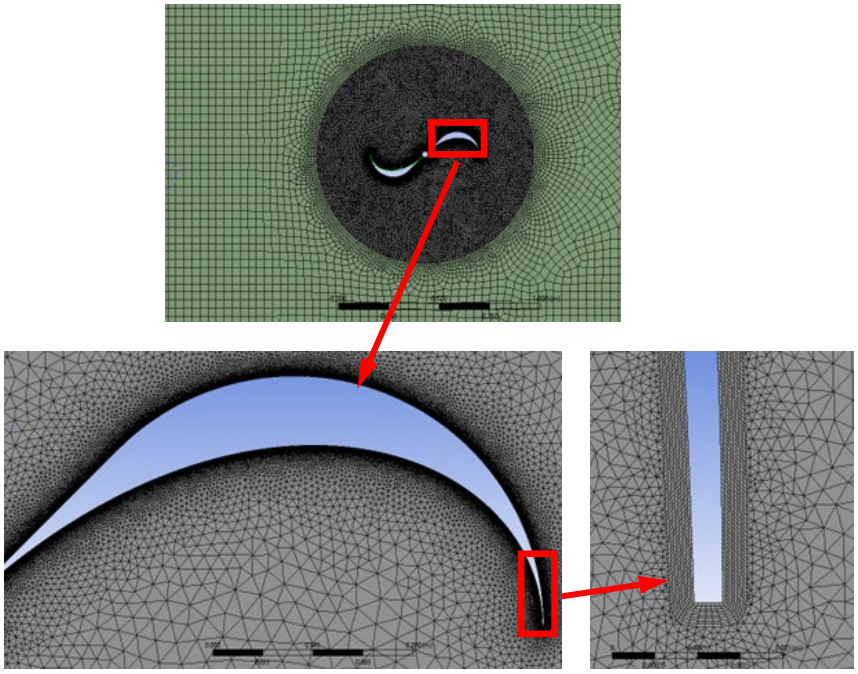

Figure 6. Grid structure around and in vicinity of the rotor of the combined Savonius wind turbine.

5. RESULTS AND DISCUSSION

5.1 CFD Model Validation and Choice of Turbulence Model

The mesh size for different computational fluid zones was chosen after carrying out a grid independence analysis on both rotating and stationary zones. Details of such analysis can be found in author's pervious work; Reference [9]. In order also to ensure the validity of current computational findings, results of the current numerical calculations were compared with the current experimental results. A suitable turbulence model was thereafter chosen based on a comparison of computational results of a few turbulence models with current experimental measurements. The tested turbulence models were the RNG k-ε, the realizable k-ε and the SST k-ω models. Figure 7 compares the numerical and experimental average power coefficient of the Bach type blade test model as a function of tip speed ratio. The available experimental domain of tip speed ratio was between 0.4 and 1.0. The computational average power coefficient was calculated by taking the average torque coefficient of the seventh revolution of the turbine rotor.

As depicted in Figure 7, the CFD model generally over predicts the power coefficients when compared to the experimental results. The reason for this behavior may be that the experimental free jet air velocity distribution over the turbine rotor was not entirely uniform as supposed in computational study. Besides, the use of two-dimensional computational domain instead of three-dimensional one may contribute to the deviation between the experimental and computational results. Despite this deviation, the numerical results are predicted with an acceptable accuracy when compared to the experimental measurements. Figure 7 illustrates that using the realizable k-ε turbulence model shows a fairly good agreement with current experimental results, as trends and magnitudes of both of the data match moderately well. The average error of each turbulence model was 11.25% for the RNG k-ε, 4.5% for the realizable k-ε and 9.6% for the SST k-ω. Demonstrating the closest results to the experimental measurements, the realizable k-ε turbulence model was used in the present computational study to model the turbulence quantities.

5.2 Turbine Performance

Figures 8 and 9 compare the turbine performance of the investigated test models, both computational and experimental ones. Torque and power coefficients in relation to the tip speed ratio are used to describe the turbine performance. The investigated computational range of tip speed ratio was set between 0.1 and 1.1. The computational results presented in each of Figure 8 and Figure 9 were acquired after computationally completing seven full revolutions of the turbine rotor. As illustrated in Figure 8, the LIUB blade exhibits to some extent higher performance parameters than the Bach type blade. Among the tested rotors, the combined blade shows the highest performance at higher values of tip speed ratio (where λ is greater than or equal to 0.5).

Comparing the computational torque coefficient of the three test models, Figure 8 shows that the combined rotor displays higher values of torque coefficient than the Bach and LIUB models except at lower degrees of tip speed ratio. According to the computational results shown in Figure 9, the combined blade improves the maximum power coefficient ($C_{p_{max}}$) of up to 11% compared to the Bach type blade and of up to 10.5% compared to the LIUB type blade. In addition, a value of 22% power coefficient of the combined blade was obtained at a value of λ = 1.1 with an increase of about 26.5% with respect to the Bach type rotor and with an increase of about 16.2% with respect to LIUB blade rotor. At low tip speed ratio, however, the differences between power coefficient of three test models are marginal.

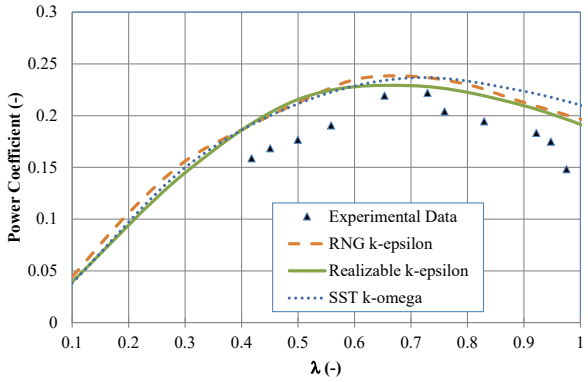

Figure 7. Power coefficient vs. tip speed ratio of Bach type rotor (BSF=1). Comparisons of present experimental data and CFD results of three turbulence models.

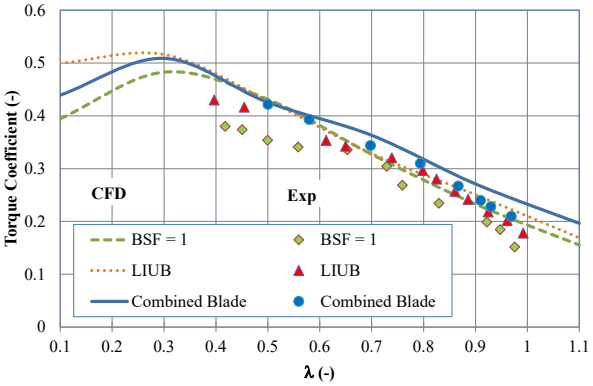

Figure 8. Comparison of present experimental and CFD torque coefficient (C_t) for Bach, LIUB and combined blade rotors.

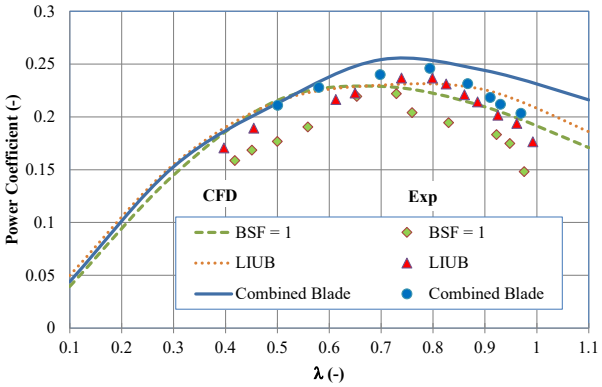

Figure 9. Comparison of present experimental and CFD average power coefficient (C_p) for Bach, LIUB and combined blade rotors.

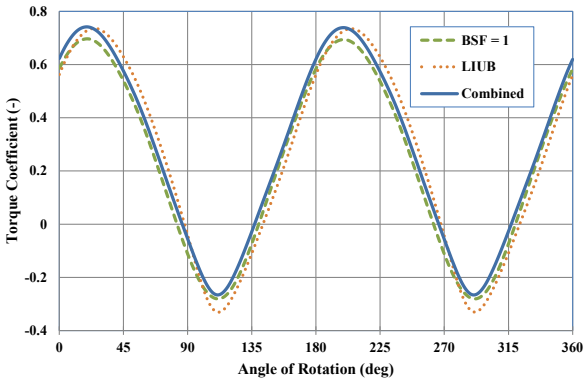

Figure 10. Comparison of instantaneous resulting computational torque coefficient at tip speed ratio of 0.9.

The increase in centroid distance of the concave side of the advancing blade, measured from the center of rotation, will increase the positive torque on the turbine rotor and consequently the output power. Whereas, decreasing the centroid distance of the convex side of the returning blade will result in a decrease in the negative torque that resists the turbine motion. Such conditions can be gained when using the combined blade rotor as the combined blade has the features of both the concave and concave sides. In this case, the resulting cyclic torque and accordingly the turbine performance will increase. The use of LIUB blade alone will improve the positive torque on the concave side while using the Bach type blade only will decrease the negative torque on the convex side.

Variation of cyclic torque coefficient with rotor angle of rotation for various rotors is illustrated in Figure 10. The torque coefficient is obtained computationally at tip speed ratio of 0.9. It has been noted that, the resulting minimum negative torque of the LIUB is improved by about 20% when applying the combined blade. Additionally, the combined rotor is driven by higher resulting positive torque at earlier angles of rotation (from 0 to 20 degrees) than the other rotors. At the same tip speed ratio, the resulting average cyclic torque coefficient is increased by 16.4% in the case of the combined blade and by 7.6% in case of the LIUB when compared to the Bach type blade.

5.3 Pressure and Velocity Distributions

Figure 11 compares the computationally calculated static pressure contours of the investigated models at λ = 0.9. Shots of static pressure contours within the rotating zone as a part of computational domain were taken at rotor angles of 0°, 45°, 90° and 135°. Bearing that the air flow enters the domain from left to right and thus the rotor rotates in counterclockwise direction. Furthermore, results were computationally achieved at a wind speed of 7 m/sec. Regions of high pressure are colored in red whilst regions of low pressure are colored in blue. In all cases and within the specified angles of rotation, the maximum pressure typically rises until the rotor angle reaches 90 deg before falling at an angle of 135 deg. As illustrated in Figure 11 at 0 deg rotating angle, the pressure downstream of the returning blade of the combined rotor is high when compared with that in the case of other models. This would reduce the negative torque acting on the returning blade and consequently would improve the turbine torque coefficient. Besides, the region of negative pressure next to the advancing blade is moderately bigger in the case of the combined blade than other models. This expects to increase the positive torque affecting this part of the blade. The

observed behavior can be attributed to the configuration's geometric profile that each rotor has and how it affects the fluctuations in local static pressure and velocity close to the wall.

Comparisons of computationally calculated velocity contours of the investigated models at $\lambda = 0.9$ are displayed in Figure 12. Velocity is color coded with red for maximum values and with blue for minimum values. As can be seen, areas with low pressure have larger velocity magnitudes. Individually, areas with greater velocity magnitudes, or lower pressure zones, are found close to the advancing blade's convex surface. This area is growing and is becoming separated from the advancing blade's leading edge as the rotating angle increases, especially as it reaches 135 deg. Furthermore, it has been found that increasing the angle of rotation is getting alongside with a rise in the maximum velocity magnitude up to an angle of 90 deg, after which it declines. As mentioned so far, the region of negative pressure next to the advancing blade of the combined blade seems to be the area of highest velocity magnitude as compared to other models.

6. CONCLUSION

The current work experimentally and computationally investigates the effects of combining two different blade shape configurations into a single blade shape design on the performance of Savonius wind turbine. Including the combined blade, three rotor blades with different configurations were experimentally and computationally tested. The combined rotor blade's outer convex surface is made like a Bach type blade profile with a particular blade shape factor, while the inner concave surface was created using a universal blade profile (LIUB). Results of computational model were compared with current experimental data and accordingly a turbulence model was chosen. Having the advantages of both of Bach and LIUB universal blade profiles, the results of turbine performance demonstrated that the combined blade performs better than other models, especially at higher tip speed ratios. Employing the combined blade rotor improves the maximum power coefficient of about 10% as compared to other rotors.

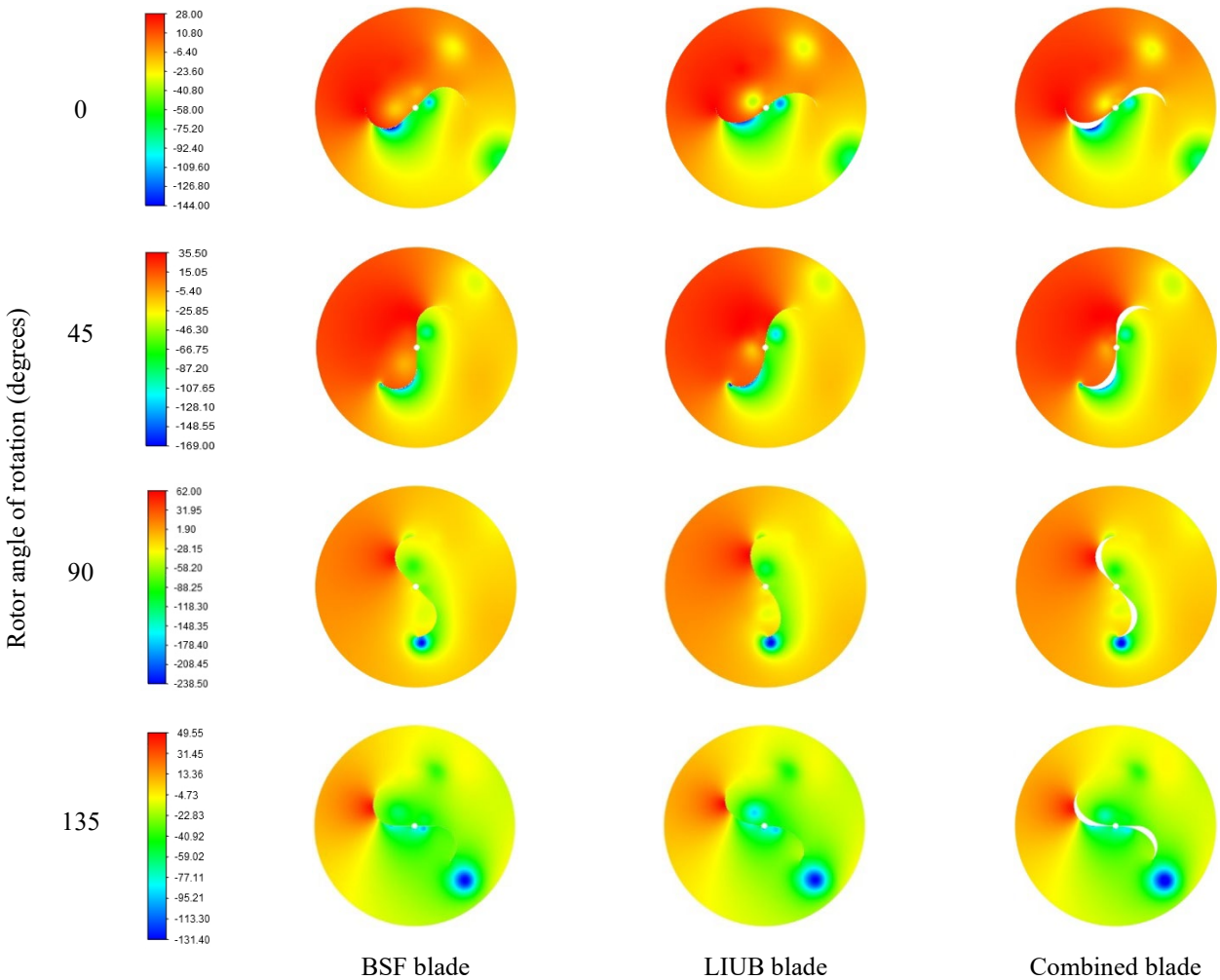

Figure 11. Static pressure contours (in Pa) for different test models at different rotor angles.

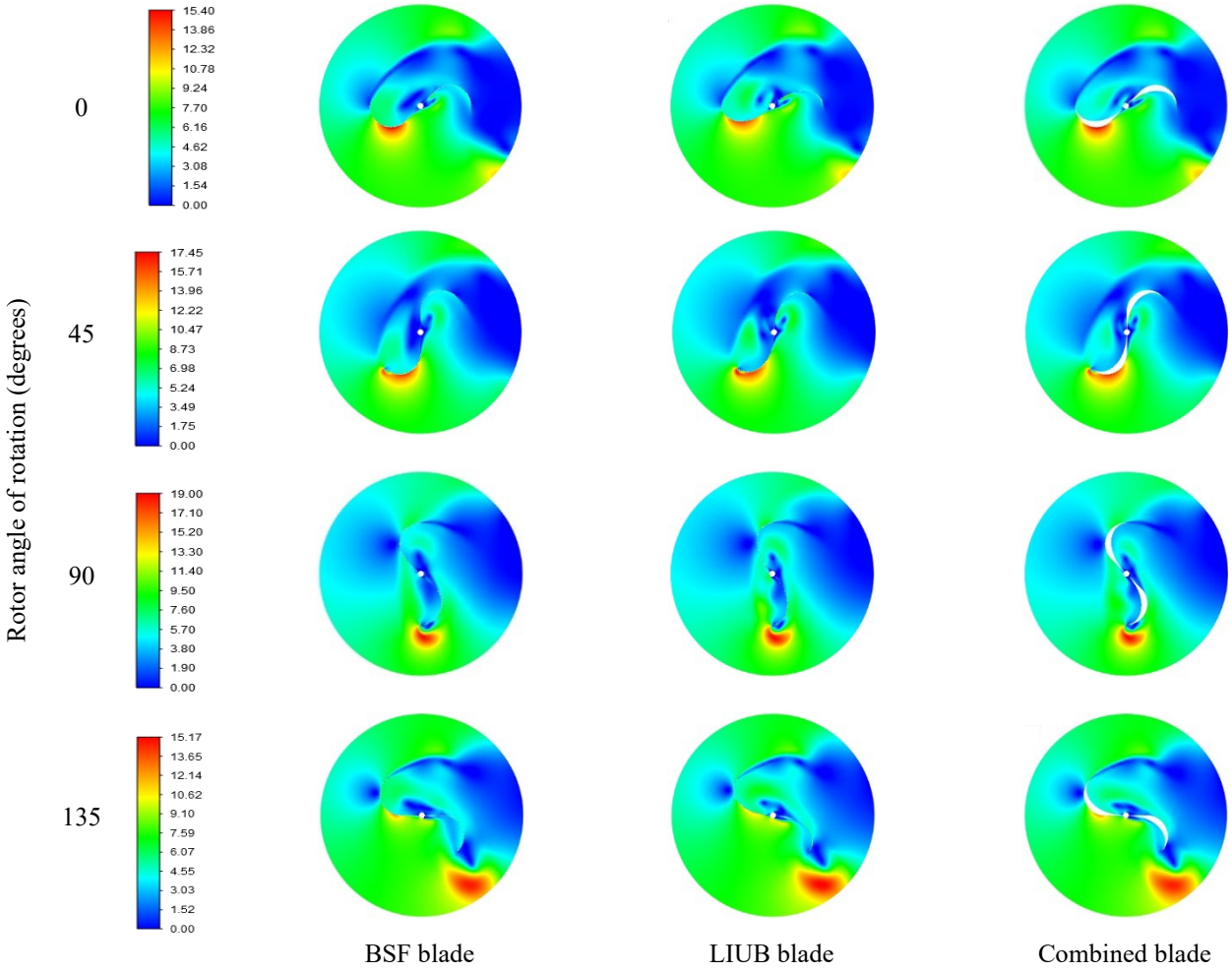

Figure 12. Velocity contours (in m/sec) for different test models at different rotor angles.

ACKNOWLEDGEMENT AND FUNDING

The author wants to thank Dr. Ismail M. Saker, Menoufia University, for his sincere support regarding the experimental test rig. The author receives no financial support for the research, authorship, and publication of this article.

DECLARATION OF CONFLICTING INTERESTS

The authors declare no potential conflicts of interest with respect to the research and publication of this article.

REFERENCES

[1] M. B. Salleh, N. M. Kamaruddin and Z. Mohamed-Kassim, The effects of deflector longitudinal position and height on the power performance of a conventional savonius turbine, *Journal of Energy Conversion and Management*, 226, 2020, 113584.

[2] M. E. Nimvari, H. Fatahian and E. Fatahian, Performance improvement of a Savonius vertical axis wind turbine using a porous deflector, *Journal of Energy Conversion and Management*, 220, 2020, 113062.

[3] K. Qasemi and L. N. Azadani, Optimization of the power output of a vertical axis wind turbine augmented with a flat plate deflector, *Journal of Energy*, 202, 2020, 117745.

[4] W. El-Askary, M. Nasef, A. Abdel-Hamid and H. Gad, Harvesting wind energy for improving performance of Savonius rotor, *Journal of Wind Engineering and Industrial Aerodynamics*, 139, 2015, 8-15.

[5] B. D. Altan and M. Atılgan, An experimental and numerical study on the improvement of the performance of Savonius wind rotor, *Journal of Energy Conversion and Management*, 49(12), 2008, 3425-3432.

[6] N. Korprasertsak and T. Leephakpreeda, CFD-based power analysis on low speed vertical axis wind turbines with wind boosters, *Journal of Energy Procedia*, 79, 2015, 963-968.

[7] N. Korprasertsak and T. Leephakpreeda, Analysis and optimal design of wind boosters for vertical axis wind turbines at low wind speed, *Journal of Wind Engineering Industrial Aerodynamics*, 159, 2016, 9-18.

[8] W. El-Askary, A. S. Saad, A. M. AbdelSalam and I. Sakr, Investigating the performance of a twisted modified Savonius rotor, *Journal of Wind Engineering and Industrial Aerodynamics*, 182, 2018, 344-355.

[9] A. -F. Mahrous, Computational fluid dynamics study of a modified Savonius rotor blade by universal consideration of blade shape factor concept, *Journal of Advanced Research in Fluid Mechanics and Thermal Sciences*, 85(1), 2021, 22-39.
[10] C. M. Chan, H. Bai and D. He, Blade shape optimization of the Savonius wind turbine using a genetic algorithm, *Journal of Applied energy*, 213, 2018, 148-157.
[11] A. Damak, Z. Driss and M. Abid, Experimental investigation of helical Savonius rotor with a twist of 180, *Journal of Renewable Energy*, 52, 2013, 136-142.
[12] M. Kamoji, S. B. Kedare and S. Prabhu, Experimental investigations on single stage modified Savonius rotor, *Journal of Applied Energy*, 86(7-8), 2009, 1064-1073.
[13] A. S. Saad, I. I. El-Sharkawy, S. Ookawara and M. Ahmed, Performance enhancement of twisted-bladed Savonius vertical axis wind turbines, *Journal of Energy Conversion and Management*, 209, 2020, 112673.
[14] U. Saha and M. J. Rajkumar, On the performance analysis of Savonius rotor with twisted blades, *Journal of Renewable Energy*, 31(11), 2006, 1776-1788.
[15] L. Chen, J. Chen and Z. Zhang, Review of the Savonius rotor's blade profile and its performance, *Journal of Renewable and Sustainable Energy*, 10(1), 2018, 013306.
[16] N. Alom and U. K. Saha, Influence of blade profiles on Savonius rotor performance: Numerical simulation and experimental validation, *Journal of Energy Conversion and Management*, 186, 2019, 267-277.
[17] K. Kacprzak, G. Liskiewicz and K. Sobczak, Numerical investigation of conventional and modified Savonius wind turbines, *Journal of Renewable Energy*, 60, 2013, 578-585.
[18] T. Zhou and D. Rempfer, Numerical study of detailed flow field and performance of Savonius wind turbines, *Journal of Renewable Energy*, 51, 2013, 373-381.
[19] H. A. H. Saeed, A. M. N. Elmekawy and S. Z. Kassab, Numerical study of improving Savonius turbine power power coefficient by various blade shapes, *Alexandria Engineering Journal*, 58, 2019, 429-441.
[20] A. Sanusi, S. Soeparman, S. Wahyudi and L. Yuliati, Experimental study of combined blade Savonius wind turbine, *International Journal of Renewable Energy Research,* 6(2), 2016, 614-619.
[21] A. M. Abdelsalam, W. A. El-Askary, M. A. Kotb and I. M. Sakr, Experimental study on small scale horizontal axis wind turbine of analytically-optimized blade with linearized chord twist angle profile, *Energy*, 216, 2021, 119304.
[22] I. M. Sakr, M. A. Abdel-Mordy, A. M. Abdelsalam and K. A. Ibrahim, Numerical and experimental investigation of the ducted wind turbine performance with and without obstacle plates, *ERJ. Engineering Research Journal*, 46(1), 2023, 21-31.
[23] ANSYS Fluent, *Fluent 15.0 User's Guide*, Fluent Incorporated, Lebanon, NH, 2015.
[24] A. -F. Mahrous, A computational fluid dynamics study of an integrating savonius-darrieus vertical axis wind turbine, *Journal of Advanced Research in Fluid Mechanics and Thermal Sciences*, 75(1), 2020, 21-37.
[25] M. Nasef , W. El-Askary, A. Abdel-Hamid and H. Gad, Evaluation of Savonius rotor performance: Static and dynamic studies, *Journal of Wind Engineering and Industrial Aerodynamics*, 123, 2013, 1-11.
[26] W. Tian, Z. Mao, B. Zhang and Y. Li, Shape optimization of a Savonius wind rotor with different convex and concave sides, *Renewable Energy*, 117, 2018, 287-299.
[27] B. Zhang, B. Song, Z. Mao, W. Tian, B. Li and B. Li, A novel parametric modeling method and optimal design for Savonius wind turbines, *Energies*, 10(3), 2017, 301.